Geophysical Research Letters

RESEARCH LETTER
10.1029/2019GL083990

Observational Evidence for Two Modes of Coupling Between Sea Surface Temperatures, Tropospheric Temperature Profile, and Shortwave Cloud Radiative Effect in the Tropics

S. Fueglistaler[1,2]

[1]Department of Geosciences, Guyot Hall, Princeton University, Princeton, NJ, USA , [2]Program in Atmospheric and Oceanic Sciences, Sayre Hall, Princeton University, Princeton, NJ, USA

Key Points:
- Average SST and difference between the warmest waters and the average ($SST^{\#}$) control tropical tropospheric temperature profile and SWCRE
- Observational evidence for pattern effect (encapsulated by $SST^{\#}$) on climate sensitivity as previously noted in GCM simulations
- Observations driven by ENSO have lagged phase of $SST^{\#}$ to Niño 3.4 index; forcing on $SST^{\#}$ may change global average temperature

Correspondence to:
S. Fueglistaler,
stf@princeton.edu

Citation:
Fueglistaler, S. (2019). Observational evidence for two modes of coupling between sea surface temperatures, tropospheric temperature profile, and shortwave cloud radiative effect in the tropics. *Geophysical Research Letters*, *46*, 9890–9898. https://doi.org/10.1029/2019GL083990

Received 3 JUN 2019
Accepted 2 AUG 2019
Accepted article online 07 AUG 2019
Published online 20 AUG 2019

Abstract Tropical average shortwave cloud radiative effect (SWCRE) anomalies observed by CERES/EBAF v4 are explained by observed average sea surface temperature ($\overline{SST}$) and the difference between the warmest 30% where deep convection occurs and $\overline{SST}$ ($SST^{\#}$). Observed tropospheric temperatures show variations in boundary layer capping strength over time consistent with the evolution of $SST^{\#}$. The CERES/EBAF v4 data confirm that associated cloud fraction changes over the colder waters dominate SWCRE. This observational evidence for the "pattern effect" noted in General Circulation Model simulations suggests that $SST^{\#}$ captures much of this effect. The observed sensitivities ($dSWCRE/d\overline{SST} \approx 1.8 W \cdot m^{-2} \cdot K^{-1}$, $dSWCRE/dSST^{\#} \approx -4.8 W \cdot m^{-2} \cdot K^{-1}$) largely reflect El Niño–Southern Oscillation. As El Niño develops, $\overline{SST}$ increases and $SST^{\#}$ decreases (both increasing SWCRE). Only after the El Niño peak, $SST^{\#}$ increases and SWCRE decreases. $SST^{\#}$ is also relevant for the tropical temperature trend profile controversy and the discrepancy between observed and modeled equatorial Pacific SST trends. Causality and implications for future climates are discussed.

1. Introduction

Changes in the climate system are commonly normalized by the associated change in global average surface temperature change, and the widely used concept of climate sensitivity uses the definition of global average surface temperature change in response to a forcing. Similarly, climate feedbacks in General Circulation Models (GCMs) may be determined through a uniform increase in sea surface temperatures (SSTs; Cess & Potter, 1988). Indeed, coupled atmosphere-ocean GCMs predict a fairly homogeneous surface temperature change in particular over the oceans in response to radiative forcing. However, it is increasingly recognized that a range of observations suggest that additional degrees freedom need to be considered. Here, we argue that open questions regarding the cloud impact on climate sensitivity (the "pattern effect", Andrews et al., 2018; Andrews & Webb, 2018; Ceppi & Gregory, 2017; Silvers et al., 2018; Stevens et al., 2016; Zhou et al., 2016) are related to the controversy surrounding the question whether the tropical tropospheric temperature trend profile follows moist adiabatic scaling (Flannaghan et al., 2014; Po-Chedley & Fu, 2012; Santer et al., 2005). That is, both depend on the question whether the temperature difference between the warmest regions with atmospheric deep convection and the tropical average remains constant under climate change. Flannaghan et al. (2014) show that since the 1980s, the Hurrell SST reconstruction (Hurrell et al., 2008) shows much stronger amplified warming of the warmest regions than the HadISST1 reconstruction (Rayner et al., 2003). Similarly, comparisons of SST trend differences focused on the cold Eastern Pacific reveal differences between coupled GCM simulations and observations, but the differences also depend on SST reconstruction and internal variability in the model simulations (e.g., Coats & Karnauskas, 2017; Zhou et al., 2016).

In the following, we show in section 2.1 that much of the observed variations in tropical average shortwave cloud radiative effect (SWCRE) as observed by CERES/EBAF v4 (Loeb et al., 2012, 2018) over the period March 2000 to March 2018 can be explained by just two parameters, $\overline{SST}$ and $SST^{\#}$, where $SST^{\#}$ is defined as the temperature of the warmest 30% minus the tropical average SST. $SST^{\#}$ is a descriptor for the evenness of the SST distribution, and similar results may be obtained with other descriptors that reflect the degree

of evenness. We use $SST^{\#}4$ because it is simple to calculate, and the SST field is the forcing for the aforementioned pattern effect. The emphasis on the warmest waters (rather than, say, coldest waters) facilitates physical intuition of the mechanism: The strong nonlocal constraint on local criticality arising from the weak temperature gradients in the tropical free troposphere (e.g., Emanuel et al., 1994; Polvani & Sobel, 2002; Sobel et al., 2002) allows the warmest regions with most deep convection to exert a strong control on the tropical average-free tropospheric temperature profile. By contrast, the boundary layer is in direct contact with the underlying surface, and consequently, the tropical average SST and the tropical average boundary layer over the ocean are tightly coupled. It follows that the tropical average boundary layer capping (reflecting the difference between average boundary layer and average-free tropospheric temperature) is related to the difference between the SST in the warmest regions with deep convection and the tropical average SST, and $SST^{\#}$ is an index thereof that can be calculated from the SST field alone.

In sections 2.2–2.4 we provide observational support for the underlying mechanistic model connecting $SST^{\#}$ and tropical cloudiness. Specifically, consistency is shown between variations in SWCRE and cloud cover as reported by CERES/EBAF v4, variations in tropical tropospheric stability in ERA-Interim reanalysis data (Dee et al., 2011), and the SSTs inferred from the CERES/EBAF v2.8 surface fluxes product (results with other SST reconstructions are very similar). The reduction to only two free parameters is facilitated by casting the problem in terms of frequency distributions rather than geographical patterns. Shifts of patterns in geographic space lead to large local anomalies of opposite sign that generally preclude conclusive attribution of the net effect (e.g., Radley et al., 2014). Sobel et al. (2002) stressed the importance of distinguishing convective from nonconvective regions and analyzed changes over time in the frequency distribution of SSTs. In section 2.3 we explain why our conclusions concerning SST frequency distributions differ from theirs.

The importance of the temperature difference between warmest regions and the average for low clouds is also emphasized by Miller (1997). Their model study seeks to predict the differential warming of the warmest regions following radiative forcing in order to predict the cloud radiative effect response and its impact on climate sensitivity. By contrast, the observational evidence presented here over the period covered by CERES/EBAF v4 is based on *observed* SST variations that are largely associated with El Niño–Southern Oscillation (ENSO; section 2.5). We therefore conclude in section 3 with a brief discussion of causality and forcing versus feedback and of implications for future and past climate states where the relation between $SST^{\#}$ and $\overline{SST}$ may be driven by processes other than the transient oscillations between El Niño and La Niña.

2. Results

All analyses are carried out with monthly mean data, and "tropical" refers to the latitude range 30° South to 30° North. The analysis of cloud radiative effect is restricted to the period March 2000 to March 2018 for which CERES/EBAF v4 data are currently available. The SWCRE is defined as the upwelling shortwave radiative flux under clear-sky conditions minus that under all sky conditions, at the top of the atmosphere. Thus, a negative SWCRE anomaly corresponds to an increase in reflected solar radiation (i.e., a cooling tendency) and *vice versa*. A simple 6-month running mean low-pass filtering is applied to reduce the noise of the monthly mean CERES/EBAF v4 data.

2.1. The Observed Tropical SWCRE Variations

Figure 1a shows the deseasonalized tropical average SWCRE as reported by CERES/EBAF v4. The figure further shows the results of two linear regressions: a linear regression of the observed SWCRE variations against $\overline{SST}$ and a multiple linear regression against $\overline{SST}$ and $SST^{\#}$. Adding $SST^{\#}$ roughly doubles the explained variance in SWCRE compared to the linear regression against $\overline{SST}$ only, giving a high correlation of $r = 0.8$ ($r^2 = 0.64$). Visual inspection shows that the most prominent variations in SWCRE are captured with the exception of the period 2003–2004. Also, we note that with the inclusion of $SST^{\#}$ the SWCRE and the SST signals are largely in-phase, a point we will return to in section 3.

The parameter $SST^{\#}$ is a crude estimator for the subcloud moist static energy in the regions of deep convection relative to the tropical average. A separation of the domain according to some threshold applied to the midtropospheric vertical wind field (Bony & Dufresne, 2005; Zhou et al., 2016) or taking precipitation as an estimator of convective activity (Flannaghan et al., 2014; Fueglistaler et al., 2015; Sobel et al., 2002) may provide a more precise descriptor. However, the point here is that the relation with SWCRE is very robust and can be captured without additional information that may not be always available (e.g., rainfall distribution before the satellite era) and may suffer from observational (rainfall) and model biases (vertical wind field).

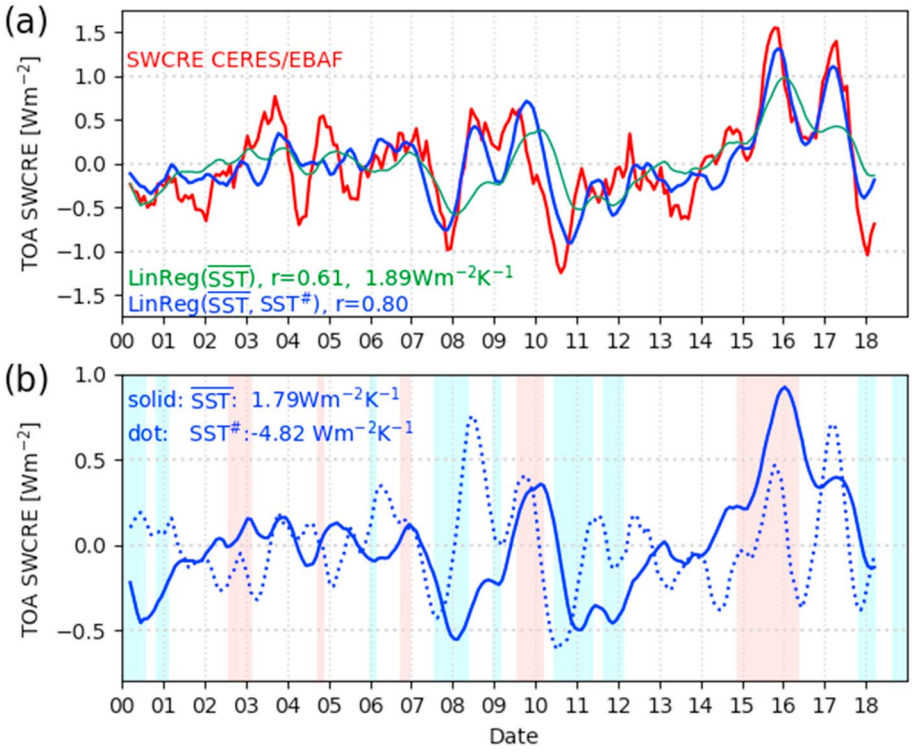

Figure 1. (a) CERES/EBAF v4 tropical average (deseasonalized) SWCRE; tropical average SST ($\overline{SST}$) scaled with slope from linear regression against SWCRE and the same for the multiple linear regression with $\overline{SST}$ and SST$^{\#}$ as predictors. (b) The time series of $\overline{SST}$ (solid line) and SST$^{\#}$ (dotted line) multiplied with their slopes dSWCRE/d$\overline{SST}$ and dSWCRE/dSST$^{\#}$ of the multiple linear regression. Correlation coefficients and slopes determined for low-pass filtered data (6-month running mean) as shown. Periods where the low-pass filtered Nino 3.4 index exceeds ±0.6 are highlighted in light red (El Niño situation) and light cyan (La Niña situation). SWCRE = shortwave cloud radiative effect; TOA = top of atmosphere; SST = sea surface temperature.

The two predictors $\overline{SST}$ and SST$^{\#}$ are not orthogonal by construction. Over the period studied here, their correlation is marginal ($r \approx 0.07$). Correspondingly, the sensitivity of SWCRE to $\overline{SST}$ changes only slightly when introducing SST$^{\#}$ to the linear regression. For the multiple linear regression, we get an increase in SWCRE (i.e., an increase in absorbed solar radiation) with average warming of dSWCRE/d$\overline{SST}$ $\approx$ 1.8 Wm^{-2}K^{-1} and a decrease in SWCRE (i.e., a decrease in absorbed solar radiation) with an increase of SST$^{\#}$ of dSWCRE/dSST$^{\#}$ $\approx$ -4.8 Wm^{-2}K^{-1}, as shown in Figure 1b. The sensitivity of SWCRE to tropical average SST of $\approx$ 1.8 W·m^{-2}·K^{-1} agrees well with that to local SST as reported by Klein et al. (2017; their Figure 3b). The magnitude of dSWCRE/dSST$^{\#}$ depends somewhat on the low-pass filtering applied. Over the period considered here, variations in SST$^{\#}$ are predominantly associated with ENSO, and the 6-month timescale for the running mean is a compromise between noise reduction and preservation of the ENSO signal. The connection of $\overline{SST}$ and SST$^{\#}$ to ENSO clearly visible in Figure 1b is further discussed in section 2.5, and the question of causality between SWCRE, $\overline{SST}$, and SST$^{\#}$ is discussed in section 3.

2.2. The Mechanism

The mechanism underlying the previous multiple linear regression builds on the expectation that the tropical average boundary layer temperature is closely tied to $\overline{SST}$, while the tropical average-free tropospheric temperature is closely tied to SSTs in the warmest regions with atmospheric deep convection (Flannaghan et al., 2014; Fueglistaler et al., 2015; Sobel et al., 2002; Zhang, 1993). To be precise, the relation is for subcloud moist entropy, but over the ocean the latter forms a fairly compact, monotonic relation with SSTs and we may use SST as proxy for subcloud moist entropy. The parameter SST$^{\#}$ thus is expected to affect the tropical average boundary layer capping strength, which in turn is known to affect low-level cloudiness in particular over the colder oceanic regions (Bretherton, 2015; Klein & Hartmann, 1993; Klein et al., 2017; Myers & Norris, 2016; Qu et al., 2014, 2015, Wood & Bretherton, 2006; Wood, 2012).

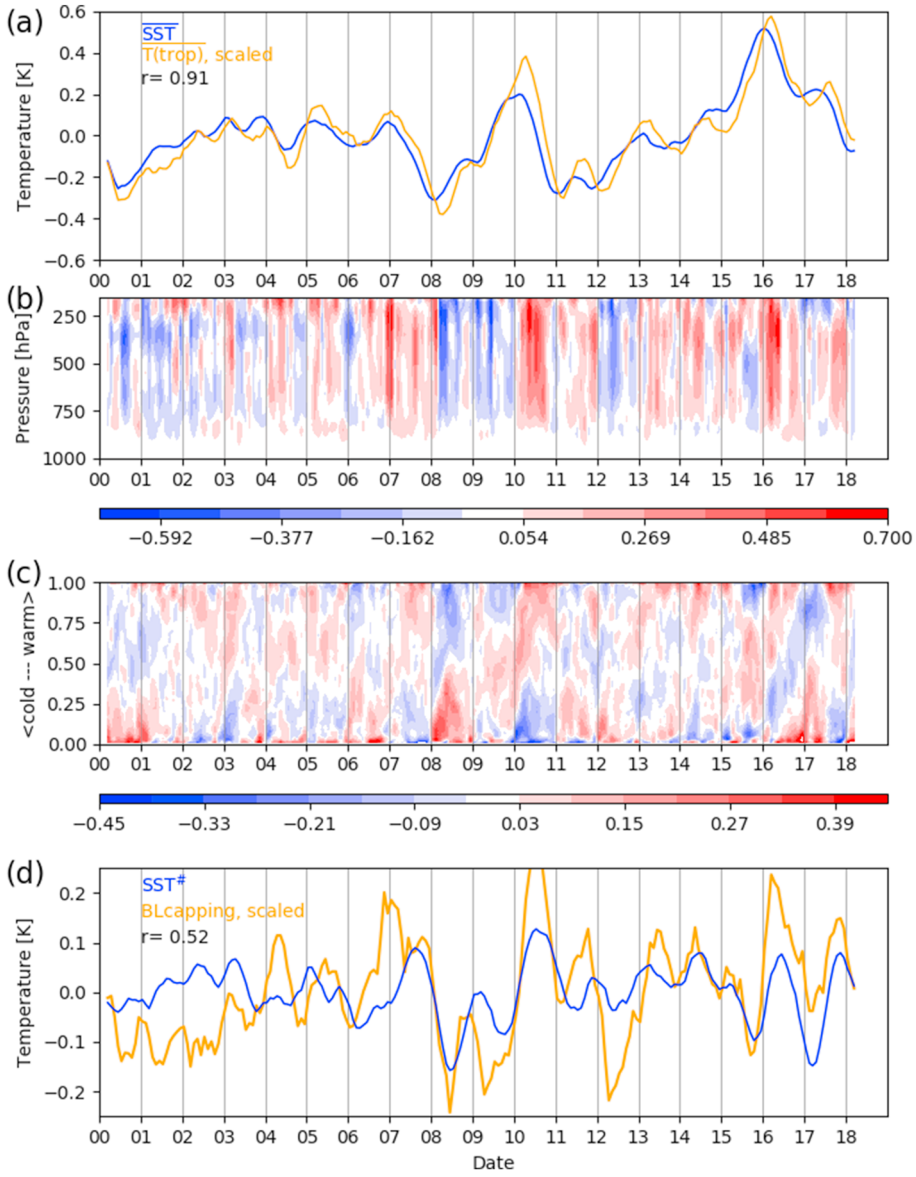

Figure 2. (a) Tropical average deseasonalized $\overline{SST}$ (blue) and tropospheric air (orange, 1,000- to 200-hPa average) temperature (in Kelvin); low-pass filtered with 6-month running mean. (b) Monthly mean residual of deseasonalized tropical average tropospheric temperature (in Kelvin) after subtracting the climatological mean scaling with tropical average boundary layer (1,000–925 hPa) temperature. The white contour of the color bar is centered at 0. (c) Tropical monthly mean SST (in Kelvin) distribution in equal area percentiles from coldest to warmest, deseaonalized and tropical average (blue line in panel a) subtracted. The white contour of the colorbar is centered at 0. (d) Time series of 6-month running means of $SST^{\#}$ (blue, difference between warmest 30% and tropical average) and variations in boundary layer capping strength not related to $\overline{SST}$ (orange, departure from climatological scaling as shown in panel b, averaged from 700 to 600 hPa). Scaling of capping strength given by linear regression against $SST^{\#}$ ($r = 0.52$).

We do not seek to directly relate the "boundary layer capping strength" to commonly used metrics such as the "lower-tropospheric stability" (Klein & Hartmann, 1993) or the "estimated inversion strength" (Wood & Bretherton, 2006). Rather, we simply assume that the stability is affected by changes in the temperature difference between boundary layer and free troposphere in a two-layer sense. By connecting the latter to $SST^{\#}$, we introduce a (global) closure assumption for the temperature above the boundary layer (typically at 700 hPa; see Klein & Hartmann, 1993) required by the above metrics of tropospheric stability. An anomalously high $SST^{\#}$ thus corresponds to an anomalously strong boundary layer capping and consequently more clouds and a negative SWCRE as is observed in Figure 1. The sensitivity of the cloud field to $\overline{SST}$ reflects

stability changes within the boundary layer with temperature, as well as other bounday layer parameters related to surface temperature (such as moisture and radiative fluxes) known to affect the cloud field.

In the following, we demonstrate that the observed tropical average boundary layer capping strength as represented in the ERA-Interim reanalysis (Dee et al., 2011) provided by the European Centre for Medium-range Weather Forecast (similar results are obtained with MERRA-2 provided by NASA Rienecker, 2011) indeed follows $SST^{\#}$ as determined from the CERES/EBAF v2.8 surface flux data product. Over the period 2000–2018, the differences between different SST reconstructions emphasized by Flannaghan et al. (2014) with respect to trends play a secondary role, and results (not shown) with the HadISST1 data (Rayner et al., 2003) are very similar.

Figure 2a shows that the observed tropical average tropospheric temperature and $\overline{SST}$ are highly correlated, in line with the notion discussed in the introduction of a unique, compact relation between the average surface temperature and any other domain-averaged variable. However, indications of a residual with non-stationary phase are visible. In order to demonstrate that the tropical temperature profile indeed has a second mode in addition to coherent temperature variations over the entire depth of the troposphere, we subtract the expected scaling with average boundary layer temperature. That is, we perform a linear regression of the deseasonalized temperature profile against the boundary layer average (here taken to be 1,000–925 hPa) deseasonalized temperature. The resulting climatological mean scaling profile closely follows the moist adiabatic scaling (not shown). The resulting residual, that is, the departure from the climatologically expected scaling with the average boundary layer temperature, is shown in Figure 2b.

We note that above about 200 hPa these residuals are likely affected by the temperature shift in ERA-Interim caused by the introduction of COSMIC/GPS temperature data over the year 2006 (Fueglistaler et al., 2013). Also, we find that the same residuals determined from GCM simulations (not shown) are more coherent throughout the free troposphere than those in ERA-Interim shown in Figure 2b. These caveats likely rooted in observational uncertainties notwithstanding, the temperature residuals in ERA-Interim show distinct phases when the free troposphere is warmer or colder than expected from scaling with average boundary layer temperature. We average these residuals over the pressure range 700 to 600 hPa to obtain a robust estimate of the implied variation in boundary layer capping strength. Figure 2d shows (Figure 2c discussed below) that these variations in boundary layer capping strength not related to average SST are indeed correlated to $SST^{\#}$ ($r = 0.52$ for 6-month running mean low-pass filtered data). Using only the 700-hPa level that is used for the lower-tropospheric stability (Klein & Hartmann, 1993) and the estimated inversion strength (Wood & Bretherton, 2006) indexes yields similar results, with slightly lower correlations due to more noise.

2.3. The Leading Mode of Tropical SST Variations

Sobel et al. (2002) performed an Empirical Orthogonal Function (EOF) analysis of the observed SST frequency distribution time series and found that the leading mode is an approximately uniform temperature change. In contrast, our analysis emphasizes the importance of $SST^{\#}$, that is, nonuniform temperature changes. Inspection of the time series of the SST frequency distribution (Figure 2c) shows why the two studies arrive at different conclusions. In Figure 2c we describe the SST distribution in terms of the average SST in equal area bins upon sorting by SST. While less common than the standard frequency distribution, this representation is more straightforward to interpret. We then deseasonalize the data and further subtract the domain-averaged anomaly (shown in Figure 2a). The resulting residuals shown in Figure 2c thus reveal the departure from uniform warming or cooling, and $SST^{\#}$ is the average of this residual over the warmest 30% of the total tropical ocean. We note prominent seesaws between warm and cold areas, for example, in the years 2007–2010 and 2016–2017, and it is these periods that give the correlation between $SST^{\#}$ and SWCRE. While an EOF analysis in the percentile space employed here captures some of that nonuniform behavior (i.e., the leading mode is not a uniform temperature change), it is evident that a substantial fraction of variance does not follow a stationary phase relation between the area bins. For reasons beyond the scope of this paper, an EOF analysis in SST frequency distribution space as employed by Sobel et al. (2002) maps most of the departure from uniform warming onto several higher-order EOFs that individually explain only little variance.

2.4. Clouds Over the Colder Waters

Figure 3 confirms that the tropical average SWCRE variations shown in Figure 1 are dominated by variations in oceanic low-level clouds and that the variations in boundary layer capping strength induced by $SST^{\#}$ affect their fractional area coverage. Figure 3a shows that the tropical average SWCRE largely follows the SWCRE

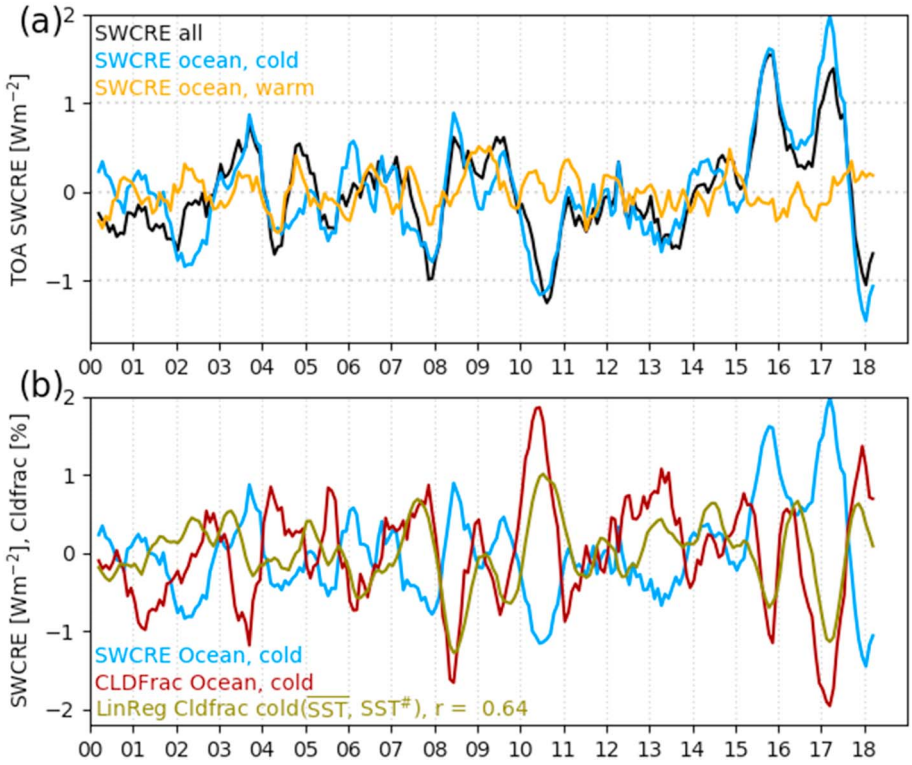

Figure 3. (a) Deseasonalized SWCRE as reported by CERES/EBAF v4 for the tropics as a whole (black), for the coldest 70% of the tropical oceanic subdomain (blue), and for the warmest 30% of the tropical oceanic subdomain (red). The oceanic anomalies are multiplied by their respective area fraction (i.e., the sum of the two anomalies shown gives the total oceanic anomaly); no scaling for ocean fraction of total tropics is applied. (b) SWCRE (blue, as in panel a) and cloud fraction (Cldfrac, in percent) as reported by CERES/EBAF v4 (brown) over the coldest 70% of the oceanic subdomain. A multiple linear regression of this cloud fraction against $\overline{SST}$ and SST$^{\#}$ (olive) yields a correlation of $r = 0.64$. SWCRE = shortwave cloud radiative effect; TOA = top of atmosphere; SST = sea surface temperature.

in the "colder" 70% of the tropical oceans, with deviations noted in the early 2000s which also show less agreement between SWCRE and the prediction based on $\overline{SST}$ and SST$^{\#}$ (see Figure 1a). Figure 3b shows that over the colder oceanic regions SWCRE and the observed cloud fraction as reported by the CERES/EBAF v4 data agree well, with a sensitivity of SWCRE to cloud fraction of about −1 W/m^2 per 1% increase in cloud fraction, in agreement with previously published values (e.g., Klein & Hartmann, 1993). The variations in cloud fraction over the colder oceanic regions in turn are also quite well explained by $\overline{SST}$ and SST$^{\#}$ ($r = 0.64$).

2.5. ENSO

Figure 1b shows that over the period of available observations, much of the variance in SWCRE, $\overline{SST}$, and SST$^{\#}$ is related to ENSO. Broadly speaking, during the La Niña situations $\overline{SST}$ is colder (increasing cloudiness), and during the El Niño situations $\overline{SST}$ is higher (decreasing cloudiness). Conversely, over the course of the 2009/2010 and 2015/2016 El Niño situations SST$^{\#}$ induces a transition from positive SWCRE (decreased cloudiness) to negative SWCRE (increased cloudiness) in the decay phase. The exceptionally strong El Niño of 1997/1998 shows an evolution of $\overline{SST}$ and SST$^{\#}$ similar to that of the 2009/2010 and 2015/2016 El Niño situations. While no CERES/EBAF v4 data are available for that period, we use the 1997/1998 El Niño due to its strong signal to exemplarily discuss the evolution of $\overline{SST}$ and SST$^{\#}$ and their impact on tropospheric temperatures.

Figure 4a shows the deseasonalized tropical average tropospheric temperature profile from January 1997 to January 1999. Figure 4c shows the Niño 3.4 index over the same period, peaking in December 1997 (El Niño) and subsequently reaching a local minimum (La Niña). Comparison of the Nino 3.4 index with the temperature profile (Figure 4a) shows that the well-established lag in tropospheric warming relative to Nino 3.4 (e.g.,

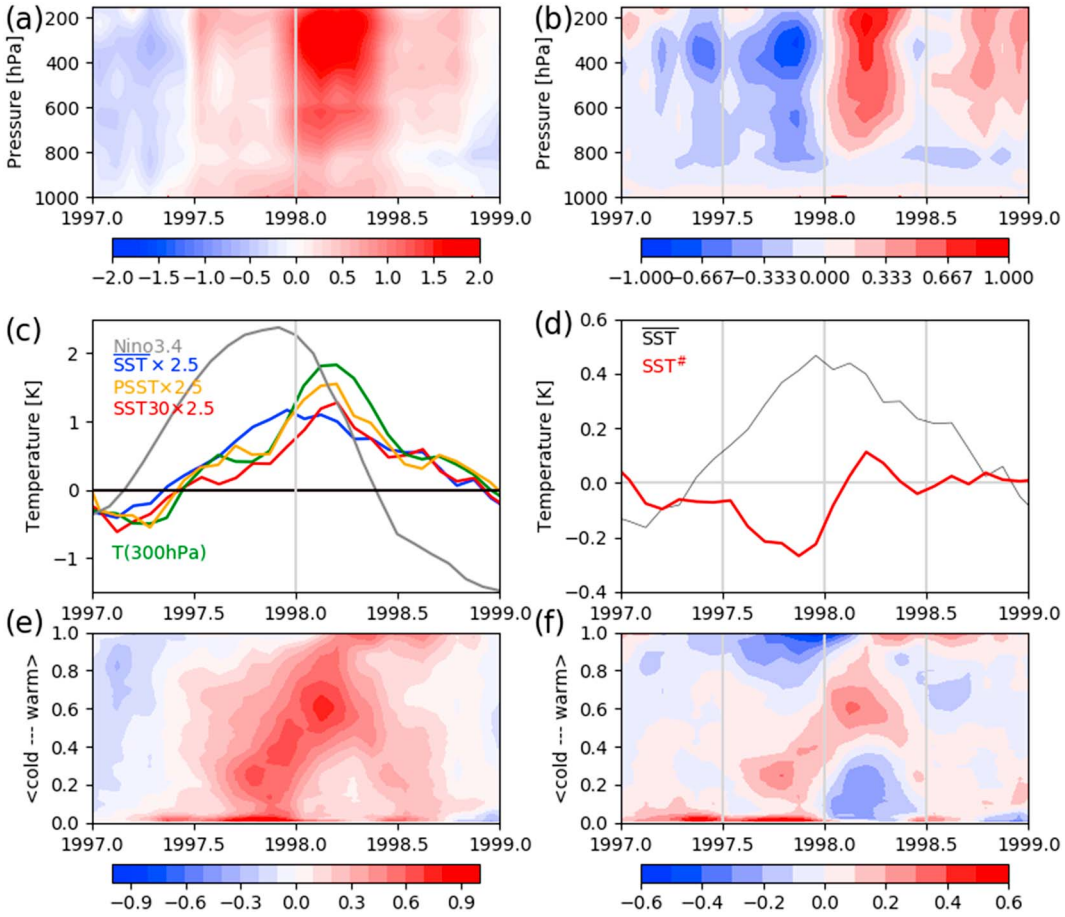

Figure 4. The 1997/1998 El Niño case study. Atmospheric temperature data from ERA-Interim, SST data from HadISST1, and precipitation from GPCP (Huffman et al., 2001); data deseasonalized over the period 1990–2010. (a) Deseasonalized tropical average tropospheric temperature (in Kelvin). (b) Deseasonalized tropical average atmospheric temperature after subtracting the climatological mean scaling with average boundary layer temperature (as in Figure 2b). (c) Nino 3.4 index (gray), air temperature at 300 hPa (green), and tropical average SST (blue), precipitation weighted SST (orange), and warmest 30% (red). The latter three are multiplied with the approximate moist adiabatic scaling factor of 2.5 to show quantitative agreement with the 300-hPa air temperature. (d) Deseasonalized tropical average SST (gray) and SST$^{\#}$ (red). (e) Deseasonalized tropical SST distribution (in Kelvin) in equal area bins of sorted SSTs. (f) Deseasonalized tropical SST distribution as in Figure 4e, after subtracting the tropical average anomaly (as in Figure 2c). SST = sea surface temperature.

Kumar & Hoerling, 2003) is largely due to the signal in the free troposphere. The residual from expected scaling with average boundary layer shown in Figure 4b (as in Figure 2b) confirms the visual impression from Figure 4a that during the peak of Nino 3.4 the free troposphere is anomalously cold and afterward anomalously warm relative to the boundary layer. Figure 4c shows that the warming at 300 hPa is delayed compared to the Niño 3.4 index but is well explained (both in terms of phase and magnitude) by the SSTs (here taken from HadISST1) in the convective region determined either by SST$^{\#}$ (red line) or precipitation-weighting (orange line; Flannaghan et al., 2014) of the HadISST1 data with rainfall from GPCP v2 (Huffman et al., 2001). Figure 4d shows that the evolution of SST$^{\#}$ recovers the tropospheric temperature deviation from expected scaling with average boundary layer temperature shown in Figure 4b, with a weaker boundary layer capping at the onset of El Niño and a stronger boundary layer capping as El Niño decays. Finally, Figures 4e and 4f show the evolution of the SST distribution (in terms of average SST in equal area bins), with and without the domain average anomaly (i.e., Figure 4f corresponds to Figure 2c).

Thus, as an El Niño situation builds up, $\overline{\text{SST}}$ and the boundary layer warm up in tandem. However, the warmest, convective regions of the ocean do not warm at the same rate. Consequently, during the peak El Niño situation SST$^{\#}$ is anomalously cold which induces a weakening of the boundary layer capping strength. In this phase, both SST$^{\#}$ and *overline* SST reduce the tropical average cloudiness (i.e., a positive

SWCRE anomaly). During the subsequent decay of El Niño, $\overline{SST}$ is still high (inducing reduced cloudiness) but $SST^{\#}$ is now also large and correspondingly has an antagonistic effect on cloudiness.

3. Discussion and Outlook

We have demonstrated that in addition to the average SST, the difference between average and the warmest waters with deep convection in the atmosphere plays a key role for climate. This difference, for which we have used $SST^{\#}$ as a proxy, controls variations in the tropical average boundary layer capping strength by controlling the average temperature difference between the boundary layer and overlying free troposphere. With low-level clouds particularly over the colder waters being sensitive to boundary layer capping strength, $SST^{\#}$ exerts a control on tropical average albedo not related to average surface temperature. This simple mechanistic picture is based on casting the tropics in terms of a distribution of states grouped by SSTs. In this frame of reference, the tropical average shortwave cloud radiative effect is formulated as a function of two thermodynamic state variables ($\overline{SST}$ and $SST^{\#}$) rather than the traditional geographic patterns with emphasis on East-West gradients in the equatorial Pacific and the Walker cell and Hadley cell circulations. Indeed, $SST^{\#}$ may be a useful parameter to encapsulate the net effect of previously noted changes in these circulations and patterns (e.g., Coats & Karnauskas, 2017; Funk & Hoell, 2015; Meehl et al., 2013; Vecchi et al., 2006; Zhou et al., 2016).

In order to quantify the sensitivity of tropical cloud albedo, we have used an ordinary linear regression with the SST parameters as predictors. Hence, we have implicitly assumed that the cloud field is forced by $\overline{SST}$ and $SST^{\#}$, rather than the cloud field forcing the SSTs. Lutsko (2018) argue that at ENSO periods, the decrease in cloudiness seen in CMIP5 models amplifies the surface temperature response. Our analysis shows that a substantial part of the initial decrease in cloudiness is due to the lagged warming of the warmest waters, thus initially decreasing the average boundary layer capping strength and hence cloudiness.

From the perspective of climate change, the question is whether $\overline{SST}$ controls $SST^{\#}$, such that the effect of $SST^{\#}$ on SWCRE would constitute a positive/negative feedback if $SST^{\#}$ decreases/increases with an increase in $\overline{SST}$. The negative low cloud feedback proposed by Miller (1997) arises from their idealized model's prediction that $dSST^{\#}/d\overline{SST} > 0$. The differences in trends of $SST^{\#}$ between different reconstructions of observed SSTs thus induce not only uncertainty regarding the tropical temperature trend profile (Flannaghan et al., 2014) but also for climate sensitivity estimates and the question of causality between $\overline{SST}$ and $SST^{\#}$. It is conceivable that $SST^{\#}$ is not only dependent on $\overline{SST}$ but that some process in the global climate system can act as a forcing on $SST^{\#}$. In this situation, the associated cloudiness change would force $\overline{SST}$, with a positive feedback (if the $dSWCRE/d\overline{SST}$ observed here is not restricted to ENSO variability) from the cloud change following a change in $\overline{SST}$. Consequently, all else being equal, a climate state with more uniform tropical SSTs (smaller $SST^{\#}$) has fewer low-level clouds and hence has a higher average surface temperature.

Data Availability

All data used in this study are publicly available in repositories maintained by the data providers as listed in the Acknowledgments section. All data postprocessing steps are straightforward averaging and linear regressions as described in the text.

Acknowledgments
S. F. would like to thank the constructive reviews from anonymous reviewers and Marcia Baker and Levi Silvers for helpful feedback on an early version of this paper. S. F. acknowledges support from the National Science Fund Awards AGS-1417659 and AGS-1743753. S. F. thanks the following agencies for generously providing free access to their data: the European Centre for Medium-range Weather Forecast (ECMWF) for providing the ERA-Interim reanalysis data, the data used here were downloaded online (https://www.ecmwf.int/en/forecasts/datasets/archive-datasets/reanalysis-datasets/era-interim); the U.K. Met Office and the Hadley Centre for providing the HadISST data, downloaded online (https://www.metoffice.gov.uk/hadobs/hadisst); NASA for providing the MERRA-2 reanalysis data, the data used here were downloaded online (https://disc.gsfc.nasa.gov); and NASA for providing the CERES/EBAF v4 data, which was downloaded online (https://ceres.larc.nasa.gov/compare_products.php). The GPCP data were provided by the NASA/Goddard Space Flight Center's Mesoscale Atmospheric Processes Laboratory, which develops and computes the 1DD as a contribution to the GEWEX Global Precipitation Climatology Project. Data set accessed online (ftp://meso.gsfc.nasa.gov/pub/).

References

Andrews, T., Gregory, J., Paynter, D., Silvers, L., Zhou, C., Mauritsen, T., et al. (2018). Accounting for changing temperature patterns increases historical estimates of climate sensitivity. *Geophysical Research Letters*, *45*, 8490–8499. https://doi.org/10.1029/2018GL078887

Andrews, T., & Webb, M. J. (2018). The dependence of global cloud and lapse rate feedbacks on the spatial structure of tropical Pacific warming. *Journal of Climate*, *31*(2), 641–654.

Bony, S., & Dufresne, J.-L. (2005). Marine boundary layer clouds at the heart of tropical cloud feedback uncertainties in climate models. *Geophysical Research Letters*, *32*, L20806. https://doi.org/10.1029/2005GL023851

Bretherton, C. (2015). Insights into low-latitude cloud feedbacks from high-resolution models. *Philosophical Transactions of the Royal Society A*, *373*, 20140415. https://doi.org/10.1098/rsta.2014.0415

Ceppi, P., & Gregory, J. (2017). Relationship of tropospheric stability to climate sensitivity and Earth's observed radiation budget. *Proceedings of the National Academy of Sciences*, *114*, 13,126–13,131. https://doi.org/10.1073/pnas.1714308114

Cess, R. D., & Potter, G. L. (1988). A methodology for understanding and intercomparing atmospheric climate feedback processes in general circulation models. *Journal of Geophysical Research*, *93*(D7), 8305–8314. https://doi.org/10.1029/JD093iD07p08305

Coats, S., & Karnauskas, K. (2017). Are simulated and observed twentieth century tropical Pacific sea surface temperature trends significant relative to internal variability? *Geophysical Research Letters*, *44*, 9928–9937. https://doi.org/10.1002/2017GL074622

Dee, D., Uppala, S., Simmons, A., Berrisford, P., Poli, P., Kobayashi, S., et al. (2011). The ERA-interim reanalysis: Configuration and performance of the data assimilation system. *Quarterly Journal of the Royal Meteorological Society*, *137*, 553–597.

Emanuel, K., Neelin, J., & Bretherton, C. (1994). On large-scale circulations in convecting atmospheres. *Quarterly Journal of the Royal Meteorological Society*, *120*(519), 1111–2157.

Flannaghan, T. J., Fueglistaler, S., Held, I. M., Po-Chedley, S., Wyman, B., & Zhao, M. (2014). Tropical temperature trends in Atmospheric General Circulation Model simulations and the impact of uncertainties in observed SSTs. *Journal Geophysical Research: Atmospheres*, *119*, 13,327–13,337. https://doi.org/10.1002/2014JD022365

Fueglistaler, S., Liu, Y. S., Flannaghan, T. J., Haynes, P. H., Dee, D. P., Read, W. J., et al. (2013). The relation between atmospheric humidity and temperature trends for stratospheric water. *Journal of Geophysical Research: Atmospheres*, *118*, 1052–1074. https://doi.org/10.1002/jgrd.50157

Fueglistaler, S., Radley, C., & Held, I. M. (2015). The distribution of precipitation and the spread in tropical upper tropospheric temperature trends. *Geophysical Research Letters*, *42*, 6000–6007. https://doi.org/10.1002/2015GL064966

Funk, C., & Hoell, A. (2015). The leading mode of observed and CMIP5 ENSO-residual sea surface temperatures and associated changes in Indo-Pacific climate. *Journal of Climates*, *28*, 4309–4329. https://doi.org/10.1175/JCLI-D-14-00334.1

Huffman, G. J., Adler, R. F., Morrissey, M. M., Bolvin, D. T., Curtis, S., Joyce, R., et al. (2001). Global precipitation at one-degree daily resolution from multisatellite observations. *Journal of hydrometeorology*, *2*(1), 36–50.

Hurrell, J. W., Hack, J. J., Shea, D., Caron, J. M., & Rosinski, J. (2008). A new sea surface temperature and sea ice boundary dataset for the community atmosphere model. *Journal of Climate*, *21*, 5145–5153. https://doi.org/10.1175/2008JCLI2292.1

Klein, S., Hall, A., Norris, J., Pincus, R., & Surveys in Geophysics (2017). Low-cloud feedbacks from cloud-controlling factors: A review, *38*, 1307–1329. https://doi.org/10.1007/s10712-017-9433-3

Klein, S. A., & Hartmann, D. L. (1993). The seasonal cycle of low stratiform clouds. *Journal of Climate*, *6*(8), 1587–1606.

Kumar, A., & Hoerling, M. P. (2003). The nature and causes for the delayed atmospheric response to El niño. *Journal of Climate*, *16*, 1391–1403.

Loeb, N., Kato, S., Su, W., Wong, T., Rose, F., Doelling, D., et al. (2012). Advances in understanding top-of-atmosphere radiation variability from satellite observations. *Surveys in Geophysics*, *33*, 359–385. https://doi.org/10.1007/s10712-012-9175-1

Loeb, N., Wang, H., Su, W., Nguyen, C., Corbrett, J., Liang, V., et al. (2018). Clouds and the Earth's radiant energy system (CERES) energy balanced and filled (EBAF) top-of-atmosphere (TOA) edition-4.0 data product. *Journal of the Atmospheric Sciences*, *31*, 895–918. https://doi.org/10.1175/JCLI-D-17-0208.1

Lutsko, N. (2018). The relationship between cloud radiative effect and surface temperature variability at el Niño–Southern oscillation frequencies in CMIP5 models. *Geophysical Research Letters*, *45*, 10,599–10,608. https://doi.org/10.1029/2018GL079236

Meehl, G., Hu, A., Arblaster, J. M., Fasullo, J., & Trenberth, K. E. (2013). Externally forced and internally generated decadal climate variability associated with the interdecadal pacific oscillation. *Journal of Climate*, *26*, 7298–7310. https://doi.org/10.1175/JCLI-D-12-00548.1

Miller, R. (1997). Tropical thermostats and low cloud cover. *Journal of Climate*, *10*, 409–440.

Myers, T., & Norris, J. (2016). Reducing the uncertainty in subtropical cloud feedback. *Geophysical Research Letters*, *43*, 2144–2148. https://doi.org/10.1002/2015GL067416

Po-Chedley, S., & Fu, Q. (2012). Discrepancies in tropical upper tropospheric warming between atmospheric circulation models and satellites. *Environmental Research Letters*, *7*, 44018. https://doi.org/10.1088/1748-9326/7/4/044018

Polvani, L. M., & Sobel, A. H. (2002). The Hadley circulation and the weak temperature gradient approximation. *Journal of the atmospheric sciences*, *59*(10), 1744–1752.

Qu, X., Hall, A., Klein, S., & Caldwell, P. (2014). On the spread of changes in marine low cloud cover in climate model simulations of the 21st century. *Climate Dynamics*, *42*, 2603–2626. https://doi.org/10.1007/s00382-013-1945z

Qu, X., Hall, A., Klein, S., & DeAngelis, A. (2015). Positive tropical marine low-cloud cover feedback inferred from cloud-controlling factors. *Geophysical Research Letterss*, *42*, 7767–7775. https://doi.org/10.1002/2015GL065627

Radley, C., Fueglistaler, S., & Donner, L. (2014). Cloud and radiative balance changes in response to ENSO in observations and models. *Journal of Climate*, *27*, 3100–3113. https://doi.org/10.1175/JCLI-D-13-00338.1

Rayner, N. A., Parker, D. E., Horton, E. B., Folland, C. K., Alexander, L. V., Rowell, D. P., et al. (2003). Global analyses of sea surface temperature, sea ice, and night marine air temperature since the late nineteenth century. *Journal Geophysical Research*, *108*(D14), 4407. https://doi.org/10.1029/2002JD002670

Rienecker, M. e. a. (2011). MERRA: Nasa's modern-era retrospective analysis for research and applications. *Journal of Climate*, *24*, 3624–3648. https://doi.org/10.1175/JCLI-D-11-00015.1

Santer, B., Wigley, T., Mears, C., Wentz, F., Klein, S., Seidel, D., et al. (2005). Amplification of surface temperature trends and variability in the tropical atmosphere. *Science*, *309*, 1551–1556.

Silvers, L., Paynter, D., & Zhao, M. (2018). The diversity of cloud responses to twentieth century sea surface temperatures. *Geophysical Research Letters*, *45*, 391–400. https://doi.org/10.1002/2017GL075583

Sobel, A., Held, I., & Bretherton, C. (2002). The ENSO signal in tropical tropospheric temperature. *Journal of Climate*, *15*(18), 2702–2706. https://doi.org/10.1175/1520-0442(2002)015<2702:TESITT>2.0.CO;2

Stevens, B., Sherwood, S., Bony, S., & Webb, M. (2016). Prospects for narrowing bounds on Earth's equilibrium climate sensitivity. *Earth's Future*, *4*, 512–522. https://doi.org/10.1002/2016EF000376

Vecchi, G., Soden, B., Wittenberg, A., Held, I., Leetsma, A., & Harrison, M. (2006). Weakening of tropical Pacific atmospheric circulation due to anthopogenic forcing. *Nature*, *441*, 73–76. https://doi.org/10.1038/nature04744

Wood, R. (2012). Stratocumulus clouds. *Monthly Weather Review*, *140*, 2373–2423. https://doi.org/10.1175/MWR-D-11-00121.1

Wood, R., & Bretherton, C. (2006). On the relationship between stratiform low cloud cover and lower-tropospheric stability. *Journal Climate*, *19*, 6425–6432.

Zhang, C. (1993). Large-scale variability of atmospheric deep convection in relation to sea surface temperature in the tropics. *Journal of Climate*, *6*(10), 1898–1913.

Zhou, C., Zelinka, M., & Klein, S. (2016). Impact of decadal cloud variations on the Earth's energy budget. *Nature Geoscience*, *9*, 871–874. https://doi.org/10.1038/ngeo2828